

Charge Transport and Electrochemical Response of Poly(3,4-ethylenedioxyppyrrole) Films Improved by Noble-Metal Nanoparticles

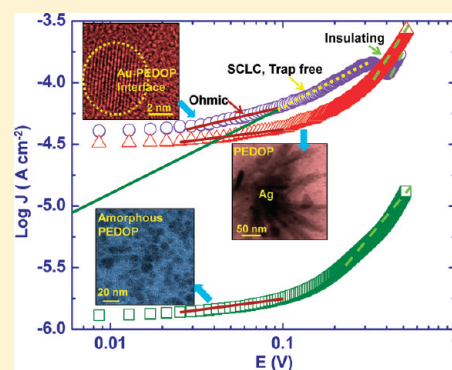
Melepurath Deepa,^{*,†} Aneeta Kharkwal,[‡] Amish G. Joshi,[‡] and Avanish Kumar Srivastava[‡]

[†]Department of Chemistry, Indian Institute of Technology Hyderabad, Ordnance Factory Estate, Yeddu-mailaram-502205, Andhra Pradesh, India

[‡]National Physical Laboratory, Dr. K. S. Krishnan Road, New Delhi-110012, India

Supporting Information

ABSTRACT: Charge-transport phenomena and redox switching of poly(3,4-ethylenedioxyppyrrole) (PEDOP) films embedded with Au and Ag nanoparticles have been investigated. In the bulk, charge transport can be described by an ohmic regime at low voltages and a space-charge-limited current regime at high voltages in PEDOP–Au, which is in contrast to trap-filled domains deduced for neat PEDOP and PEDOP–Ag nanocomposites, all indicating transitions driven by an external bias. This also allowed a direct estimation of a fairly high charge-carrier mobility at room temperature in PEDOP–Au, in addition to a higher donor density, which are advantageous for device applications. X-ray photoelectron spectroscopy and high-resolution transmission electron microscopy affirmed the prevalence of Au/Ag nanoparticles as nonleachable entities in PEDOP, thus allowing the movement of electrons through the conducting nanoparticles during electrochemical switching, an effect that is absent in the neat PEDOP film. Valence-band spectra and optical studies revealed that nanoparticles narrowed the band gap and increased the absorption coefficient of PEDOP, which enhanced the electrochromic switching ability of PEDOP. A coloration efficiency enhancement by an order of magnitude, higher electrochemical charge intercalation capacity, and higher diffusion rates reflect the role of noble-metal nanoparticles in improving the conduction and electrochemical activity of PEDOP.



1. INTRODUCTION

Conjugated polymers have attracted immense attention as electrochromic electrodes owing to their striking colors, low cost, ease of processing, high electronic conductivity, and robust switching capability.^{1,2} Of these polymers, poly(3,4-ethylenedioxyppyrrole) (PEDOP), a relatively less investigated conducting polymer, is promising for a plethora of reasons, including high contrast ratio, high visible-light transmittance and excellent conductivity in the oxidized form, and low oxidation potential, thus enabling its use in energy-efficient smart windows or dynamic displays.^{3,4} PEDOP switches from a bright red natural form to a highly transmissive blue-gray doped form.⁵ On the other hand, metal nanoparticles, because of quantum size effects, show an optical response and electronic structure that are dramatically different from their bulk behavior, and these characteristics are exploited in a variety of applications.⁶ To this end, incorporation of noble-metal nanoparticles in a conducting polymer matrix enhances the functionality of the resultant nanocomposite, as metallic nanoparticles not only improve the conduction properties of the polymer but also provide a greater number of electrochemically addressable sites for redox reaction. In the past, the synergy between the properties of a given conducting polymer (namely, fast redox switching and tunable optical modulation and electronic structure) and that of

nanoparticles (such as surface plasmon resonance) has been demonstrated for composites formed thereof.^{6,7}

In an earlier work, Li et al. prepared a composite material using 3,4-ethylenedioxythiophene (EDOT) and gold chloride, with the monomer serving as the reductant for the Au^{3+} to Au^0 conversion.⁸ In another study, Yang et al. showed the superior biocatalytic application of polyaniline/gold nanocomposites.⁹ For poly(3,4-ethylenedioxythiophene) or PEDOT, polypyrrole, and poly(3-methylthiophene), it has been successfully demonstrated that the surface of the polymer film becomes more conductive upon exposure to colloidal solutions of Au/Ag.¹⁰ Similarly, the improved electrical transport and chemical sensing properties of individual multisegmented PEDOT–Au nanowires has been explored¹¹ and cellulose whiskers coated with PEDOT–poly(styrene sulfonate) (PEDOT:PSS), were found to have high electrical conductivities.¹² In another study, Li et al. synthesized Ag, Au, and Pt nanoparticles with a reasonable size dispersity using water-dispersible conducting polymer colloids composed of polyaniline (PANI) and conventional polyelectrolytes.¹³

Received: February 1, 2011

Revised: April 26, 2011

Published: May 18, 2011

However, PEDOP-based nanocomposites have seldom been synthesized or characterized to date.

Herein, we report (i) the charge-transport phenomena in bulk and (ii) potential-dependent ion/electron transfer and propagation in nanocomposite PEDOP films, encompassing poly(*N*-vinyl-2-pyrrolidone)- (PVP-) capped Ag and Au nanoparticles, while in conjunction with an electrolyte. In this report, unlike a previous one, wherein only electrochromism was emphasized,¹⁴ we specifically examine the effect of noble-metal nanoparticles in controlling the microstructure, composition, and therefore the electronic properties of PEDOP. Heretofore unreported, electrochemical impedance spectroscopy furnished valuable insights into the role of nanoparticles in modifying the charge-transfer and diffusion processes in these devices during coloration and bleaching.

2. EXPERIMENTAL SECTION

2.1. Materials. 3,4-Ethylenedioxypyrrole (EDOP), poly(methyl methacrylate) (PMMA, $M_w = 996000$), silver nitrate (AgNO_3), gold(III) chloride solution (~ 30 wt % in dilute HCl, 99.99%) from Aldrich and poly(*N*-vinyl-2-pyrrolidone) (PVP, $M_w = 40000$) from Acros were used as received. Deionized water (resistivity $\approx 18.2 \text{ M}\Omega \text{ cm}$) obtained through Milli-Q system, ionic liquid 1-Butyl-1-methylpyrrolidinium bis(trifluoromethylsulfonyl)imide, sodium borohydride (NaBH_4), potassium hexacyanoferrate ($\text{K}_3[\text{Fe}(\text{CN})_6]$) $\text{N,N-dimethylformamide}$ (DMF) and methanol were obtained from Merck and ferric chloride (FeCl_3) was obtained from Qualigens.

2.2. Syntheses of Silver and Gold Colloids. Dissolution of 0.302 g of PVP and 0.1018 g of AgNO_3 in 8 mL of DMF yielded a clear bright yellow solution, which was irradiated discontinuously at a power of 300 W for a total duration of 90 s in a long-necked round-bottom flask, to prevent increase in pressure and spouting out of contents. The resulting colloidal solution had a purple-pink hue and showed opalescence¹⁵ and this dispersion was utilized for forming the PEDOP–Ag nanocomposite film. The solution was also subjected to irradiation for durations greater/less than 90 s, for optimization of the irradiation interval.

To a clear solution of 0.05 g of PVP prepared in 150 mL of DMF was added a solution of 0.07 g of HAuCl_4 in 10 mL of methanol with continuous stirring over a duration of 10 min. To this formulation was immediately added 0.027 g of NaBH_4 dissolved in 10 mL of methanol. An abrupt change in the color of the colloid, from yellow to wine-red, was observed, signaling the formation of Au nanoparticles.¹⁶

2.3. Deposition of PEDOP and PB Film. EDOP (0.001 M) in the ionic liquid 1-butyl-1-methyl pyrrolidinium bis(trifluoromethylsulfonyl)imide was used as the electropolymerization bath; a transparent conducting substrate ($\text{SnO}_2\text{-F}$ -coated glass, Pilkington, 14–18 Ω/sq) was employed as the working electrode, a Pt rod and Ag/Ag^+ were used as the auxiliary and reference electrodes, respectively. A constant potential of +1.5 V was applied to the working electrode for 10 min. The ensuing PEDOP films were rinsed in ethanol several times and dried in air for 2 h. Prussian blue films were grown from a solution of 10 mM $\text{K}_3[\text{Fe}(\text{CN})_6]$ and 10 mM FeCl_3 in 0.01 N HCl (in deionized water) in a two-electrode cell by galvanostatic electrodeposition by applying a fixed current density of 10 mA cm^{-2} to a $\text{SnO}_2\text{-F}$ -coated glass substrate for 8 min. The counter electrode was also a $\text{SnO}_2\text{-F}$ -coated glass substrate of the same dimensions. The as-obtained PB films were rinsed in deionized water, dried, and stored in air. PEDOP films were grown

on a Gamry Reference 600 potentiostat/galvanostat, and PB films were deposited using a Keithley 2400 current source. PEDOP films were immersed in silver and gold colloids for 2 h, to obtain PEDOP–Ag and PEDOP–Au films that were subjected to an ultrasonic rinse in neat DMF for 2 min to remove physisorbed particles and dried and stored in air in the dark.

2.4. Fabrication of Prototype Electrochromic Cells. Electrochromic devices were fabricated with neat PEDOP, PEDOP–Ag, and PEDOP–Au nanocomposite films as the cathodes, Prussian blue (PB) film as the anode, and a clear transparent gel composed of 1-butyl-1-methylpyrrolidinium bis(trifluoromethylsulfonyl)imide containing 12 wt % PMMA as the polymer electrolyte sandwiched between the two layers. An acrylic tape was used as a spacer, the entire device assembly was held in place with binder clips, and a sealant (cyanoacrylate adhesive, Perma-bond, Aldrich) was applied by running the nozzle along the four sides of the device.^{17,18} The sealant cured within a few hours at ambient temperature. After removal of the binder clips, the devices were ready for use. The approximate active geometric area of the devices was 3 cm \times 2.5 cm.

2.5. Characterization Techniques. Transmission electron microscopy (TEM) was carried out on an HRTEM Tecnai G² F30 STWIN transmission electron microscope with a field emission gun (FEG) source at 300 kV. Samples were carefully lifted from the substrate to an aqueous medium and then transferred to a carbon-coated copper grid for TEM. Surface morphological features were obtained on a scanning electron microscope (SEM, Zeiss EV MA-10) at 20 kV in secondary electron mode after a thin gold layer had been sputtered on to the film surface. Atomic force microscopy (AFM) images were recorded on a Veeco instrument in noncontact tapping mode. SEM and AFM images for all films are shown in Figures S1 and S2 (Supporting Information). X-ray photoelectron spectroscopy (XPS) data were recorded for the as-synthesized PEDOT/nanocomposite films using a Perkin-Elmer 1257 model spectrometer operating at a base pressure of 7.8×10^{-8} Torr at 300 K with a nonmonochromatized Al K α line at 1486.6 eV, an analyzer pass energy of 60 eV, and a hemispherical sector analyzer capable of 25 meV resolution. Corrections due to charging effects were applied by using C (1s) as an internal reference and the Fermi edge of a gold sample. The overall instrumental resolution was about 0.3 eV. The core-level spectra were deconvoluted using a nonlinear iterative least-squares Gaussian fitting procedure. For all fitting doublets, the full width at half-maximum (fwhm) values were fixed accordingly. The nanocomposite films were also subjected to argon sputtering, whereby up to ~ 10 nm of the top layer of the films were etched out and the Ag and Au core-level spectra were recorded for the sputtered films. The sputtering was accomplished by an argon ion beam of 4 keV energy and 20 mA emission current from a differential pumped ion gun (model 04-300) operating in raster mode at a base pressure maintained at 2×10^{-6} Torr. Absorption spectra of solutions and variation of the optical density of devices as a function of applied potential were measured on a Perkin-Elmer Lambda 25 spectrophotometer. The electronic conductivities of neat PEDOP, PEDOP–Ag, and PEDOP–Au nanocomposites were obtained by transferring the films from the substrates into a circular crater (0.5 cm in diameter) in the center of a mica sheet and sandwiching the same between two stainless steel (SS) electrodes, which in turn were insulated from one another by Teflon rings. I – V characteristics were obtained by linear sweep voltammetry (LSV) wherein the voltage was swept from –3.0 to +3.0 V

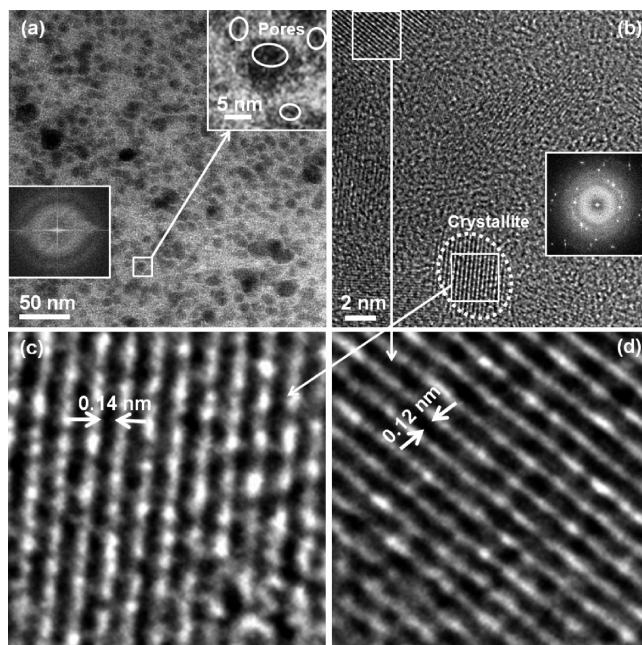


Figure 1. HRTEM images of (a) neat PEDOP (inset on right shows ultrafine pores in ellipses and inset on left shows SADP pattern of the polymer) and (b) coexisting amorphous and crystalline structures in PEDOP–Au nanocomposite (inset shows an SADP pattern from the nanocomposite). Lattice-scale images oriented along the (c) $\langle 220 \rangle$ and (d) $\langle 311 \rangle$ planes of cubic crystalline structure of Au nanoparticles.

and ac impedance spectra were recorded for the same configuration (SS/Electroactive film/SS) under a dc potential of 0 V superimposed over an ac amplitude of 10 mV, over a frequency range of from 1 MHz to 0.1 Hz. Mott–Schottky plots were recorded at a fixed frequency of 1 kHz as voltage was swept within the range from −1 to +1 V. Cyclic voltammetry (CV) for was performed for the devices, wherein PEDOP/nanocomposite was used as the working electrode and PB was employed as the counter electrode over potential ranges from −1.0 to +1.0 V and from −3.0 to +3.0 V. Electrochemical impedance spectroscopy measurements on devices were performed at different values of dc bias and fixed ac voltage of 10 mV and the devices were subjected to an equilibration time of 100 s. All electrochemical measurements for device/films were performed on a Gamry reference 600 potentiostat/galvanostat/ZRA with PHE 200/EIS 300 softwares.

3. RESULTS AND DISCUSSION

3.1. High-Resolution Transmission Electron Microscopy.

Figure 1a displays an HRTEM image of the neat PEDOP film, which shows a uniform distribution of polymer aggregates; the inset on the right-hand side is an enlarged view of one such aggregate. Nanopores of ~2–4-nm dimensions are seen (in ellipsoids), and they play a pivotal role for entrapping Ag/Au nanoparticles. The inset on the left side of the same panel shows the corresponding selected-area electron diffraction pattern (SADP), obtained by fast Fourier transformation (FFT). It is composed of concentric diffuse rings, characteristic of the amorphous nature of PEDOP. The HRTEM image of the PEDOP–Au nanocomposite film in Figure 1b shows the strong interfacial contact between Au nanoparticles and PEDOP in the

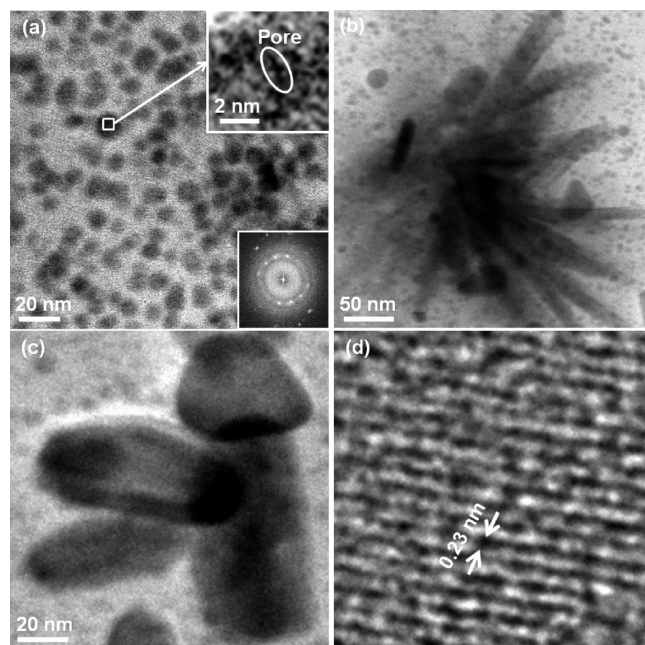


Figure 2. HRTEM images of PEDOP–Ag nanocomposite: (a) low-magnification image showing a uniform distribution of aggregated grains, (b) elongated fiberlike shapes juxtaposed with regular grains, (c) crystallites with definite grain boundaries, and (d) lattice-scale image of a Ag crystallite oriented along the $\langle 111 \rangle$ plane. The top inset in part a shows a fine pore in the film structure, and the bottom inset is an SADP pattern from the nanocomposite.

form of regions of lattice fringes corresponding to Au nanoparticles juxtaposed with the amorphous polymer. One such nanocrystal of Au is circled in a dotted line in Figure 1b. Such a structure consisting of porosity and interconnectivity (between polymer chains and also between Au and polymer) promotes (a) penetration of the electrolyte during redox switching and (b) also improves the conductivity of the polymer for both ion uptake and electron transfer, as nanoparticles are electron conduits. Because they are not completely reduced (Au^0) but have some residual charge, they also show affinity for ions. The inset of Figure 1b shows the corresponding SADP, the bright white spots arising from the crystalline planes of Au, superimposed on diffuse rings due to the polymer. The size of Au nanoparticles was found to be in the range of ~2–5 nm. The lattice-scale images chosen from two different regions of Figure 1b are shown in Figure 1c,d. In contrast to Au nanoparticles oriented along the $\langle 111 \rangle$ plane as observed earlier,²¹ herein, Au nanoparticles oriented along $\langle 220 \rangle$ and $\langle 311 \rangle$ reflections corresponding to interplanar spacings of 0.14 and 0.12 nm are observed in Figure 1c,d. These values match well with JCPDS data (04-784) of the face-centered-cubic crystalline structure of Au.

The TEM image of the PEDOP–Ag nanocomposite in Figure 2a shows quasispherical grains distributed uniformly across the film surface. In contrast to the neat film, here, the shapes of the grains are better defined, and the contrast is much sharper (inset of on the upper side of the panel). Elongated pores of ~2-nm length and 0.6-nm width can be seen in the magnified view of the dark center of one grain in Figure 2a. The SADP at the bottom left of the same panel shows a few spots due to Ag nanocrystals. Fibrous shapes (embedded in the polymer matrix) were also observed for these composite (Figure 2c), and these are

characteristic of Ag nanoparticles, as the neat PEDOP film was devoid of any such feature. The longitudinal dimension was about 75 nm, and the transverse was \sim 32 nm. Further, the UV-visible absorption spectrum of the neat Ag colloid (Figure 8a, below) also showed multiple peaks, hinting at the presence of particles with nonspherical shapes. The lattice-scale image from an Ag nanoparticle (Figure 2d) shows an interplanar spacing of 0.23 nm. This Ag nanocrystallite is oriented along the $\langle 111 \rangle$ plane, pertaining to the cubic crystalline structure of Ag, in accordance with JCPDS card 04-783.

3.2. X-ray Photoelectron Spectroscopy and Valence-Band Spectra. The XPS survey spectra of neat PEDOP, PEDOP–Ag, and PEDOP–Au nanocomposite films shows distinctive signals due to C, S, N, O, and F (Figure S3 in the Supporting Information), and in the nanocomposites, additional signals due to Ag and Au are visible. The deconvoluted C, S, and O core-level spectra of neat PEDOP, PEDOP–Ag, and PEDOP–Au nanocomposite films, after fixing the fwhm, show multiple components (Figure S4, Supporting Information). From the deconvoluted spectra, the atomic percentage contributions of C, S, and O components in PEDOP, PEDOP–Ag, and PEDOP–Au nanocomposites were deduced, and these are summarized in Tables S1 and S2 of the Supporting Information. From the atomic percentage values of $I_{\text{Ag}-\text{O}}$ and $I_{\text{Au}-\text{O}}$ (Table S2, Supporting Information), rough estimates of Ag and Au loadings in the polymer are 0.24 and 0.25, respectively. Also, the atomic percentage of $I_{\text{S}=\text{O}}$ (characteristic of imide ion) is reduced on going from neat PEDOP to PEDOP–Ag/PEDOP–Au nanocomposites, as the nanoparticles that are confined to the surface tend to lower the dopant's contribution. From the atomic ratio of $I_{\text{C-S}}/I_{\text{C}(\text{total})}$, the doping level of imide in the films was determined; for neat PEDOP, this ratio was 0.33, and for PEDOP–Ag and PEDOP–Au, it was 0.30 and 0.25, respectively. Again, the dopant levels in the nanocomposites are slightly lower than that obtained for neat PEDOP, which is indirect evidence for the tethering of Ag/Au nanoparticles with the polymer. The $I_{\text{C-O-C}(\text{polymer})}/I_{\text{S=O}(\text{dopant})}$ atomic ratio for neat PEDOP was 0.67, which shows that I_{Ag} or I_{Au} might be on the order of 0.33, which, in fact, is only slightly less than the experimentally observed $I_{\text{Ag}-\text{O}}$ and $I_{\text{Au}-\text{O}}$ values. Further confirmation for the entrenchment of Ag/Au nanoparticles in nanocomposites was obtained from the core-level spectra of Au and Ag recorded after the top 10-nm layer of each nanocomposite film was removed by argon sputtering. The spectra are shown in Figure S3 (Supporting Information). The intensities of the Ag/Au signals decreased as compared to those for the unspattered nanocomposites, but because the signals continued to be distinctive and did not vanish, this indicates that the nanoparticles were not merely confined to the surface of the PEDOP film but percolated through the cross section of the film. XPS analyses thus provided conclusive evidence for (a) Ag/Au-PEDOP interaction, (b) inclusion of the imide anions in the film, and (c) Au/Ag incorporation along the depth of the films.

The valence-band spectra, illustrating the density of states approaching the Fermi level (or zero energy), are shown in Figure 2. A comparison of parts a–c of Figure 2 shows that the PEDOP–Au nanocomposite has a markedly high intensity for density of states above the Fermi level, in contrast to neat PEDOP and PEDOP–Ag films. Incidentally, for a pristine Ag sample, in a previous report, a similar response was recorded.¹⁹ This clearly reflects the role of conducting Au nanoparticles

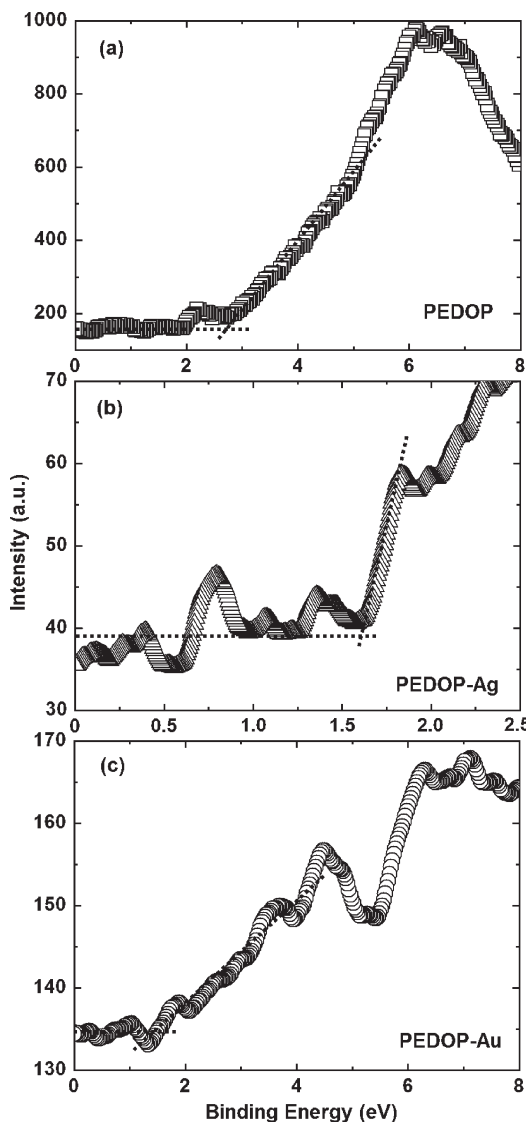


Figure 3. Valence-band spectra of (a) neat PEDOP, (b) PEDOP–Ag, and (c) PEDOP–Au nanocomposite films displaying their respective Fermi edges. The point of intersection of the dotted lines corresponds to the energy gap between the valence band and the Fermi level.

in increasing the filled-state concentration in PEDOP–Au. Furthermore, the gap from the valence band or highest occupied molecular orbital (HOMO) to the Fermi level was found to be 1.33 eV, which is smaller than that obtained for the neat PEDOP (2.66 eV) and PEDOP–Ag (1.6 eV) films. This is suggestive of a higher band gap for the latter two films, as compared to the PEDOP–Au nanocomposite. Possibly, charge carriers associated with Au nanoaparticles can introduce additional states in the band gap of the polymer, so that the experimentally observed value is lower. The opposite observation was previously made for PEDOT doped by insulating polystyrene sulfonate.²⁰ The optical gap studies also ratify this claim. Direct band gaps for the three films were determined from Tauc plots (Figure 3a–c), wherein the absorption coefficient varies as a function of photon frequency according to

$$\alpha h\nu \propto (h\nu - E_g)^{1/2} \quad (1)$$

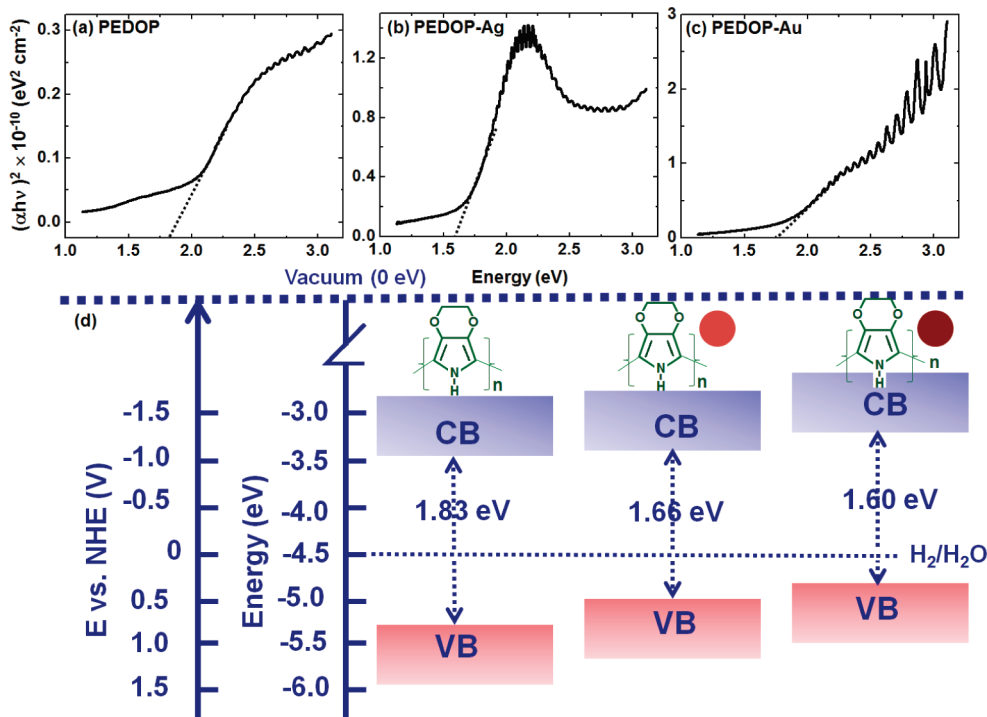


Figure 4. Main edge absorption spectra plotted as $(\alpha h\nu)^2$ versus photon energy ($h\nu$) for the (a) neat PEDOP, (b) PEDOP–Ag, and (c) PEDOP–Au films in their neutral states. (d) Approximate levels of the HOMO/VB and LUMO/CB, showing the narrowing of the direct band gap (E_g) in the composites.

where $h\nu$ is the photon energy and E_g is the direct band gap. The absorption coefficient was determined from the absorption plots using the relation

$$\alpha = \frac{1}{d} \log[I_o(\lambda)/I(\lambda)] \quad (2)$$

where d is the thickness where $\log(I_o/I)$ is the absorbance. The absorption data for the films in their most reduced or neutral state (under -2.1 V) was chosen, as we anticipate that there will not be any interference from the polaronic/bipolaronic levels, generally introduced in the gap in the oxidized or doped state. The optical band gaps of the neat film and PEDOP–Ag and PEDOP–Au nanocomposites were 1.83, 1.66, and 1.60 eV, respectively, obtained from the intercepts of the linear parts of the Tauc plots. The positions of the valence bands in Figure 3d were fixed from the HOMO level corresponding to the onset of the oxidation peak in the corresponding cyclic voltammograms; the values were normalized with respect to the H^+/H_2 redox couple. The cyclic voltammograms of the films are shown in Figure S5 (Supporting Information). The lowest unoccupied molecular orbital (LUMO) or conduction-band levels were determined by subtracting the band gap values from the corresponding HOMO levels. Although a one-to-one concurrence between the valence-band spectrum and the spectral band gap is not possible, as the former corresponds to the oxidized film and the latter to the reduced one, nevertheless, it is clear that Au nanoparticles do narrow the band gap, thus satisfying the dual requirement for a material to be a good electrochromic: high absorption coefficient and low band gap. Although the role of nanoparticles is not exactly comparable to that of electron-acceptor substituents on donor thiophene units, wherein a broadening of the spectral absorption breadth and increase in

absorption coefficients were observed as a function of increasing acceptor strength,^{21–23} nevertheless, because similar effects were induced herein, the implications might also be alike.

3.3. I–V Characteristics and Mott–Schottky Analyses. The I – V characteristics of neat PEDOP, PEDOP–Ag, and PEDOP–Au films recorded in an SS/film/SS configuration are shown in Figure 4. The Nyquist plots (Z'' versus Z') for the same films are shown in the corresponding insets. The potential window of a linear (akin to a plateau-like) response ascribable to an ohmic dependence of voltage on current is found (i) between -1 and $+1$ V for neat PEDOP, (ii) between -1.5 and $+1.2$ V for PEDOP–Ag, and (c) between -1.5 and $+0.5$ V for the PEDOP–Au nanocomposite (Figure S6, Supporting Information). The steep rise in current outside these potential windows for all three films is due to potential-activated transport of charge carriers, the onset of which occurs at high potentials. The discernible difference between the three samples is seen in the form of a peak observed at $+2.1$ V for the PEDOP–Au nanocomposite. Such a kink in the I – V curve was previously observed for a metal/poly(3-hexylthiophene) contact.²⁴ For an Al/polymer/PEDOT:PSS/In₂O₃:Sn diode,²⁵ a similar spike activated at $E > 1.9$ V was associated with a space-charge-limited current. The magnitude of current is an order of magnitude greater for the two nanocomposite films as compared to the neat polymer film in the potential range under consideration. The $\log J$ (current density) versus $\log V$ curves (Figure 5) showed a slope of ~ 1 in the low-bias region, corresponding to the ohmic regime, as discussed above. Of particular interest is the high-bias regime, which shows a curvature followed by a steep increase for the PEDOP–Ag and neat PEDOP films; the former possibly corresponds to a trap-filling regime (i.e., the rapid change experienced by current) due to a Fermi-level shift.²⁶ However,

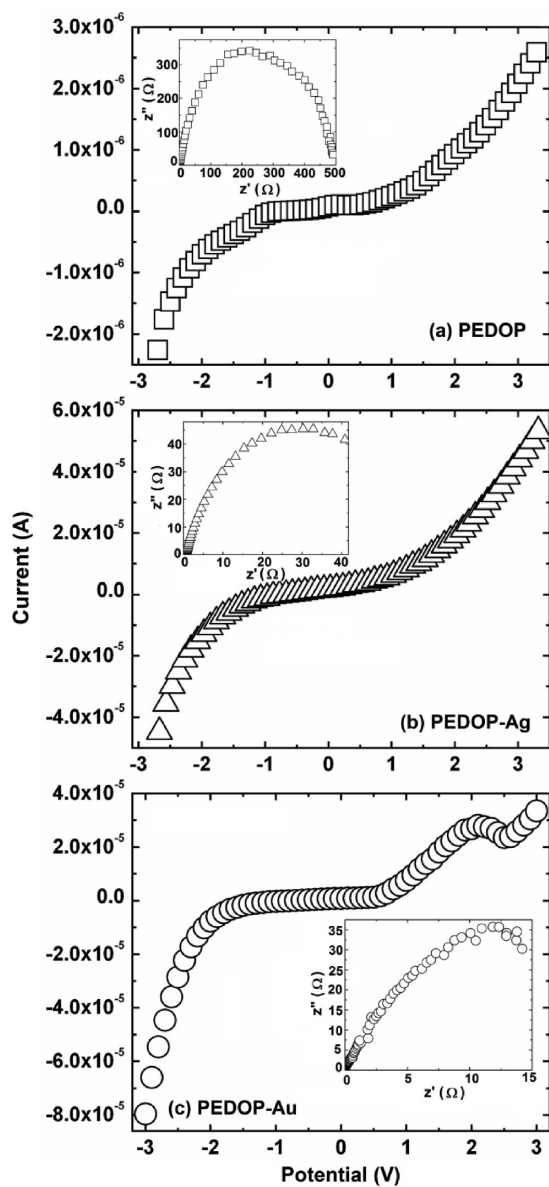


Figure 5. I – V characteristics of (a) neat PEDOP, (b) PEDOP–Ag, and (c) PEDOP–Au nanocomposites. The insets show the corresponding Nyquist (Z'' versus Z') plots for the films.

for the PEDOP–Au film, this region corresponds to a slope of slightly less than 2 and is described by the trap-free space-charge-limited current (SCLC) as it obeys the Mott–Gurney law^{26,27}

$$J_{\text{SCLC}} = \frac{9}{8} (\epsilon_r \epsilon_0 \mu V^2 / L^3) \quad (3)$$

In eq 3, ϵ_r is the dielectric constant of the nanocomposite and was determined by equating the resistance at ω_{\max} [$C = 1/(2\pi f)_{\max} R$] to the capacitance ($C = A\epsilon_0\epsilon_r/L$) (from the insets of Figure 4a–c), μ is the charge-carrier mobility, and L is the sample thickness. In the ohmic region, for all of the films, the conductive component comprises predominantly the thermally excited charge carriers as $J = ne\mu V/L$. Because we observed an almost $\log J \propto 2 \log V$ dependence only in the PEDOP–Au nanocomposite, in particular, at higher potentials attributed to SCLC, the transport in this regime is dominated by the injected

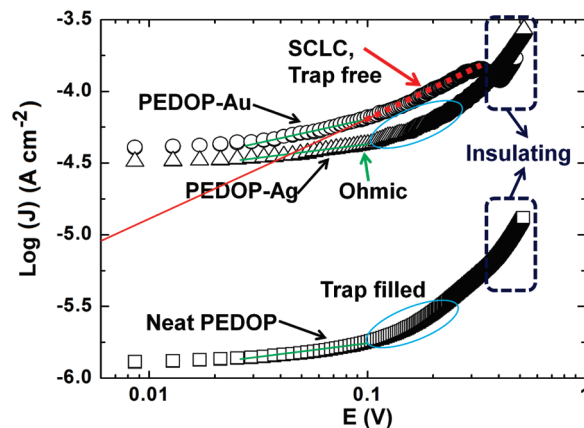


Figure 6. $\log J$ – $\log V$ plots for neat PEDOP, PEDOP–Ag, and PEDOP–Au films; the green lines correspond to the ohmic regime, and the red line shows the Mott–Gurney dependence. The blue lines enclose the trap-filled and quasi-insulating regimes.

holes controlled by space charge. From eq 3, the charge-carrier mobility in PEDOP–Au was found to be $5.6 \times 10^{-6} \text{ cm}^2 \text{ V}^{-1} \text{ s}^{-1}$, which is close to electron/hole mobilities reported for organic solar cells containing PEDOT:PSS as the hole transport layer.²⁷ At further high voltages, the conductive fraction gives way to a greater number of insulating sites with increasing voltage, and therefore, the system can be visualized as a continuum medium comprising conductive sites and an insulating phase, and this trend is common to all three of the films. Similar dependences have been observed for other conjugated polymers such as poly(3-methylthiophene).²⁸

The electronic conductivity (σ) of neat PEDOP, PEDOP–Ag, and PEDOP–Au films (insets of Figure 4a–c) was determined from the resistance at ω_{\max} to be 0.2, 1.7, and 4.1 mS cm⁻¹, respectively. The nanocomposites, by the virtue of the intimate contact that the intrinsically conducting metallic nanoparticles have with PEDOP, are characterized by higher conductivities. In an earlier report, the in situ conductivity of substituted polypyrrole was found to be in the range of 1–20 S cm⁻¹, depending on the applied potential. For a poly(alkylthiopyrrole), an in situ conductivity of 54 S cm⁻¹ was obtained.²⁹ In the present report, the values are somewhat lower, as they are for as-fabricated films and were determined under zero-biasing conditions.

Mott–Schottky plots (C^{-2} versus E) for neat PEDOP, PEDOP–Ag, and PEDOP–Au films are displayed in Figure 6. At negative potentials, in all three cases, the C^{-2} characteristic is linear (over a wide bias range), and above the flat band potential (E_{fb} obtained by extrapolation to $C = 0$), the capacitance decreases for neat PEDOP and PEDOP–Ag films. With respect to neat PEDOP ($E_{fb} = +0.64$ V), E_{fb} is shifted negatively for the PEDOP–Ag ($E_{fb} = +0.38$ V) and PEDOP–Au ($E_{fb} = +0.4$ V) nanocomposites. This shift can be attributed to the accumulation of additional charges in the surface states due to Ag/Au nanoparticles. A similar behavior was previously reported for a poly(3-hexylthiophene) system.^{24,30} The unpinning of bands by charging of surface states due to Ag/Au nanoparticles is clearly evident from these curves.

The charge-carrier density was calculated from the slopes in Figure 6, using the relation

$$1/C^2 = 2/e\epsilon\epsilon_0 N_D(E - E_{fb} - kT/e) \quad (4)$$

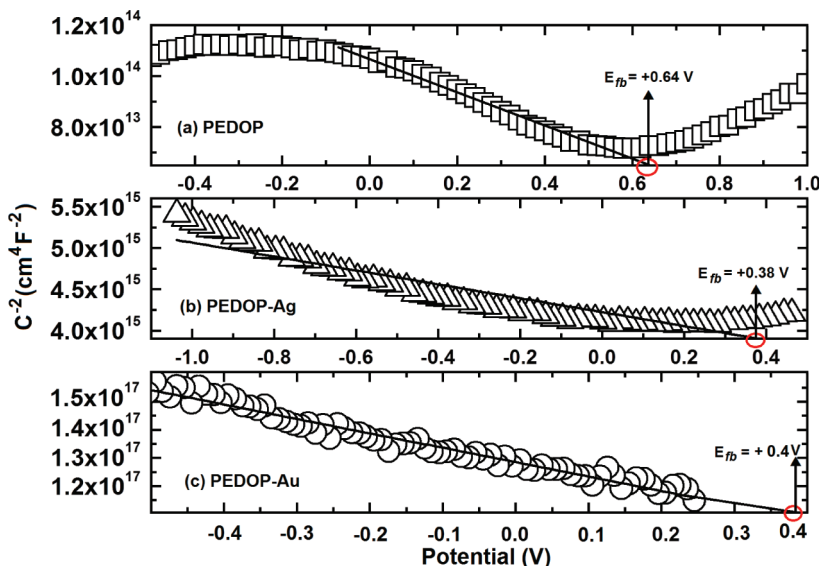


Figure 7. Mott–Schottky plots (C^{-2} versus E) for (a) neat PEDOP, (b) PEDOP–Ag, and (c) PEDOP–Au. The lines were obtained from linear fits, and the intercepts on the abscissas correspond to the flat band potentials.

where C is the capacitance of the electrode, N_D is the hole-acceptor concentration for a p-type semiconductor (PEDOP), E is the applied potential, and ϵ_0 is the permittivity of free space. C was determined from $C = 1/\omega_{\max}R$, using the insets in Figure 4. The donor density (N_D) was found to be $7 \times 10^{16} \text{ cm}^{-3}$ for neat PEDOP, and the values were higher, at 5×10^{17} and $8 \times 10^{18} \text{ cm}^{-3}$, respectively, for PEDOP–Ag and PEDOP–Au nanocomposites. The higher donor densities of the nanocomposites arise from the presence of conducting nanoparticles surrounded by more insulating regions composed of the polymer. These values are, however, lower than that reported for PEDOT ($N_D = 7 \times 10^{20} \text{ cm}^{-3}$).³¹

The oxidized PEDOP–Ag film exhibits a value of $\lambda_{\max} = 595 \text{ nm}$ (Figure S7a of the Supporting Information), and the Ag colloid used for preparing the film had a λ_{\max} value of 523 nm (shown in Figure 7). Similarly, for the oxidized PEDOP–Au film, the onset of the broad absorption extending over most of the visible region was at $\sim 550 \text{ nm}$. This was red-shifted with respect to that of the neat Au colloid, for which a broad absorption was seen in the 400–500-nm range (Figure 7). The red shift of λ_{\max} on going from neat colloid to the PEDOP–Au/Ag nanocomposite and the band gap narrowing on going from neat PEDOP to PEDOP–Au/Ag provide experimental evidence suggesting charge transfer from the noble-metal nanoparticles to the semiconducting polymer in relation to Fermi-level equilibration (as electrons will try to fill the holes in the semiconductor; shown in the inset of Figure S7b in the Supporting Information). The shrinking of E_g in the nanocomposite is possibly due to the filling of the unoccupied bands in the neat polymer (as shown in Figure S7b of the Supporting Information). Similar observations have also been made for donor–acceptor macromolecular systems.²¹ This is also supported by the higher donor density observed for the nanocomposite as compared to the neat polymer.

3.4. Absorption Spectra. The absorption spectra of Ag and Au colloids along with their digital photographs are shown in Figure 8a. The orange-red Ag colloid irradiated for 30 s showed a broad absorption peak spanning wavelengths from 500 to

700 nm, with $\lambda_{\max} = 569 \text{ nm}$. The purple solution used to prepare the PEDOP–Ag nanocomposite was obtained by 90 s of irradiation, with $\lambda_{\max} = 523 \text{ nm}$. Further irradiation for an additional 40 s yielded a bright violet solution, with $\lambda_{\max} = 550 \text{ nm}$. To prepare the nanocomposite with the polymer, we used the Ag colloid with the smallest fwhm and minimum intensity, as compared to the other two sols, so as to enable a synergistic contribution from the $\pi-\pi^*$ absorption of the polymer in neutral state and the nanoparticles. The wine-red-colored gold colloid showed a large absorption in the 400–500-nm wavelength range. The undiluted Au colloid was used for the PEDOP–Au nanocomposite film synthesis. These absorption peaks, be it Ag or Au colloid, arise from surface plasmon resonance (SPR), that is, by the excitation of surface plasmons upon interaction with incident light.³²

The absorption spectra of neat PEDOP, PEDOP–Ag, and PEDOP–Au devices as a function of applied potential are shown in Figure 8b. As expected, the neat PEDOP exhibits the least absorption change on going from +1.5 V (oxidized form) to −2.1 V (reduced form). For the PEDOP–Ag and the PEDOP–Au nanocomposites, the absorption change (ΔOD) is much higher in the entire visible region. Ag nanoparticles, nonetheless, induced a more striking effect on the absorbance of PEDOP than do Au nanoparticles. In the case of PEDOP–Ag, the SPR peak is retained, with $\lambda_{\max} = 402 \text{ nm}$ at +1.5, and at −2.1 V, it shows a blue shift to 380 nm and an intensity enhancement as well, due to contribution from the $\pi-\pi^*$ absorption of PEDOP. In contrast, for PEDOP–Au, at −2.1 V, the contribution from Au nanoparticles is indistinct, as it seems to have merged with PEDOP's absorption with $\lambda_{\max} = 500 \text{ nm}$. However, the larger optical density changes observed for both PEDOP–Ag and PEDOP–Au, in comparison to those for neat PEDOP, for the same values of applied bias, show (i) the availability of a greater number of electrochemically active sites and (ii) an efficient utilization of charges incorporated as color centers. This eventually translates into a much higher coloration efficiency for the nanocomposite films. A schematic showing the moieties in the PEDOP–Au/Ag nanocomposite and photographs of

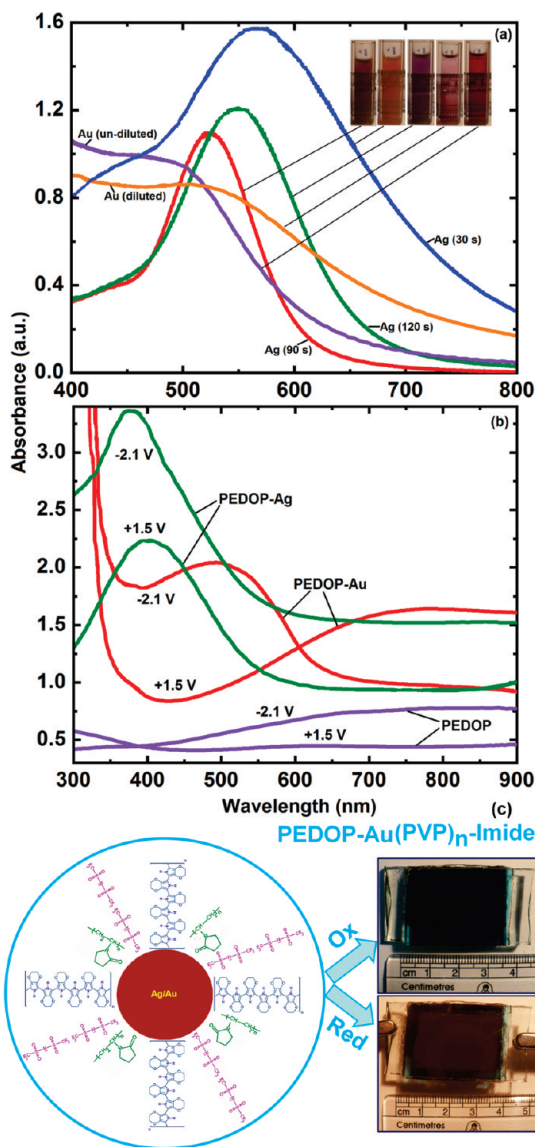


Figure 8. Absorption spectra of (a) Ag and Au colloids (with digital photographs in the insets) and (b) neat PEDOP, PEDOP–Ag, and PEDOP–Au nanocomposite-based devices recorded at +1.5 and -2.1 V in the visible region. (c) Schematic of a PEDOP–Ag or PEDOP–Au nanocomposite; the device is based on PEDOP–Au.

PEDOP–Au-PB device in the colored and bleached states are presented in Figure 8c.

The ΔOD versus charge density plots for neat PEDOP, PEDOP–Ag, and PEDOP–Au nanocomposite based devices, recorded at 550 and 633 nm, are shown in Figure 9. From the linear dependence of absorption change and intercalated charge per unit area, coloration efficiency (CE or η) was determined for the devices using the equation given below.

$$CE(\lambda) = \Delta OD(\lambda)/Q \text{ (C cm}^{-2}\text{)} \quad (5)$$

For neat PEDOP, rather low values of 72 and $13 \text{ cm}^2/\text{C}$ were obtained at 550 and 633 nm, and this could be due to high charge densities. Higher values are attainable,³ but under the experimental conditions employed, these were the values obtained. The PEDOP–Ag nanocomposite showed higher coloration efficiencies: 183 and $112 \text{ cm}^2/\text{C}$ at 550 and 633 nm, respectively.

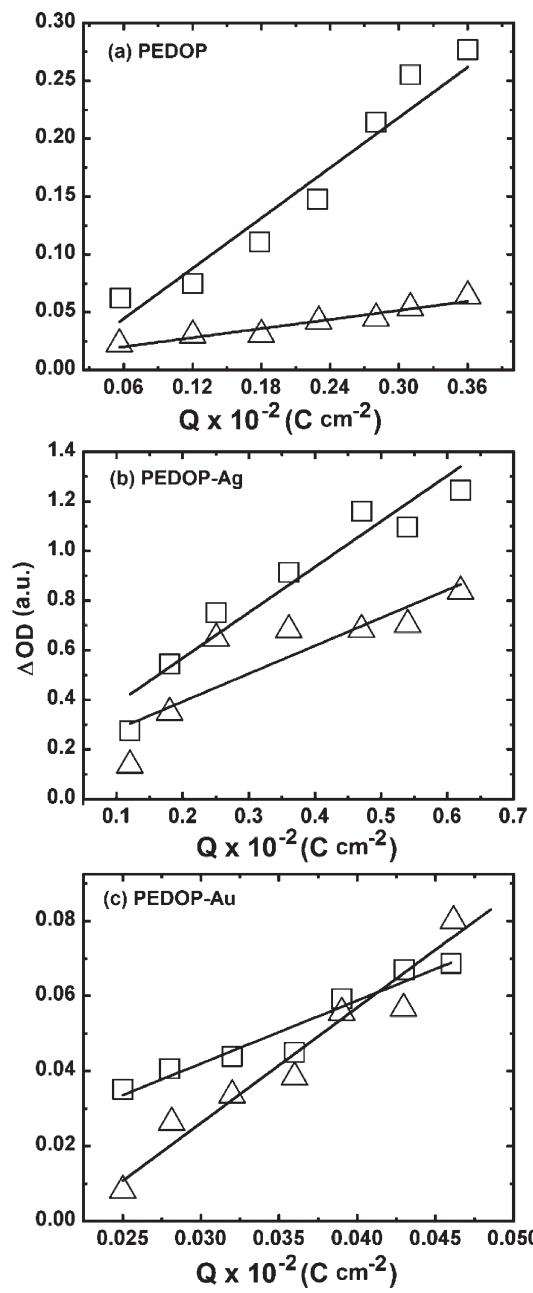


Figure 9. Absorbance change (ΔOD) versus inserted charge density plots of (a) neat PEDOP, (b) PEDOP–Ag, and (c) PEDOP–Au nanocomposite-based devices at 550 (\square) and 633 (Δ) nm. The lines represent the linear fits for coloration efficiency.

For the PEDOP–Au nanocomposite, the values were 168 and $307 \text{ cm}^2/\text{C}$ at 550 and 633 nm, respectively. No exact value of coloration efficiency has been reported for PEDOP in the literature, although absorption versus wavelength spectra under different potentials have been discussed.³ In comparison with its thiophene analogue, for PEDOT–PANI³³ and PEDOT–PB³⁴ devices, incorporating a LiClO₄-based electrolyte, coloration efficiencies of $285 \text{ cm}^2/\text{C}$ ($\lambda = 570 \text{ nm}$) and $338 \text{ cm}^2/\text{C}$ ($\lambda = 590 \text{ nm}$) were observed. In yet another report,³⁵ a composite coloring efficiency of $206 \text{ cm}^2/\text{C}$ was achieved for PEDOT at $\lambda_{\max} = 585 \text{ nm}$, for 80% of the maximum modulation. Our values agree reasonably well with the reported values. It is also

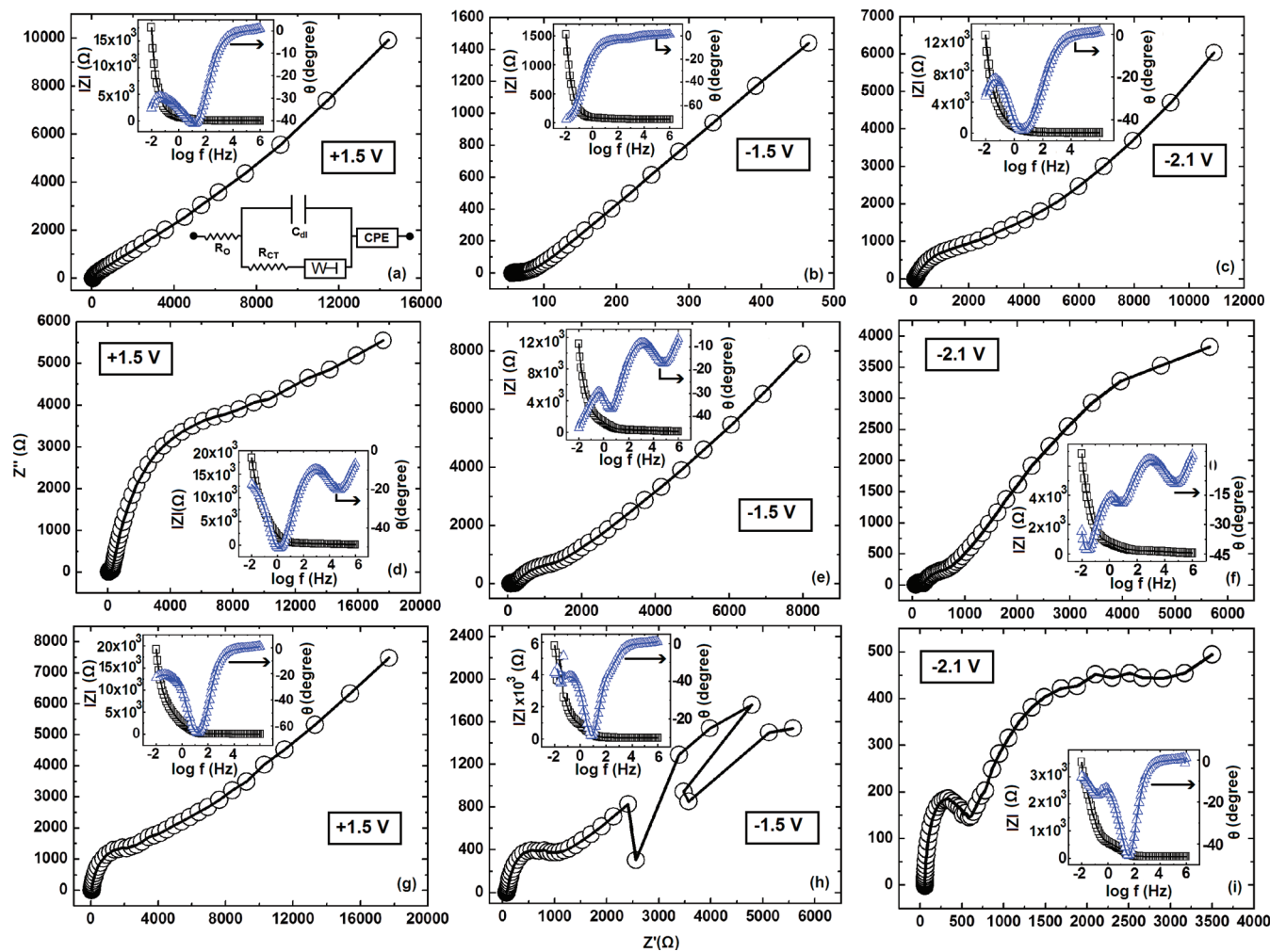


Figure 10. Nyquist plots under different dc potentials (at a fixed ac potential of 10 mV) for (a–c) neat PEDOP: (a) +1.5, (b) -1.5, and (c) -2.1 V, (d–f) PEDOP–Ag nanocomposite: (d) +1.5, (e) -1.5 and (f) -2.1 V and (g–i) PEDOP–Au nanocomposite-based devices: (g) +1.5, (h) -1.5, and (i) -2.1 V. The inset at the right-hand side of panel a shows the Randles equivalent circuit used for fitting the experimental data (\circ) in a–i; the lines represent the fits. The other insets in panels a–i display the corresponding Bode plots: (\square) $|Z|$ versus $\log(f$ Hz) and (Δ) phase angle (θ) versus $\log(f$ Hz).

noteworthy that, in contrast to the results for neat PEDOP and PEDOP–Ag, the amount of charge required to attain such a high value of coloration efficiency is almost an order of magnitude lower for the PEDOP–Au nanocomposite. This implies that a large contrast (as seen from Figure 8b) can be induced at low charge intercalation levels, which, in turn, is advantageous for maximizing the operational lifetime of the device.

3.5. Electrochemical Impedance Studies. Electrochemical impedance spectra of neat PEDOP-, PEDOP–Ag-, PEDOP–Au-based devices, recorded under dc potentials of +1.5, -1.5, and -2.1 V, are shown in Figure 10. The insets display the corresponding Bode plots, and the equivalent circuit displayed in Figure 10a gave satisfactory fits over the entire frequency range from $\sim 10^6$ to 0.01 Hz. The impedance response of the working electrode is described with a model composed of the solution resistance (R_s), the electrical double-layer capacitance (C_{dl}) in parallel with the charge-transfer resistance (R_{CT}), and a finite-length working diffusion element Z_D . The two electrodes PEDOP and PB separated by the dielectric (electrolyte) can be visualized as a nonideal capacitor, which is represented by a

Table 1. Electrochemical Impedance Spectroscopy Results for PEDOP/Nanocomposite and PB as Working Electrodes in the PEDOP/Nanocomposite–PB Device, Obtained by Fitting the Experimental Data in the Model Shown in Figure 10a

parameter	applied E (V)	neat PEDOP	PEDOP–Ag	PEDOP–Au
R_{CT} (Ω)	+1.5	842	120	30
	-1.5	68.5	560	50
	-2.1	418.5	561	180
C_{dl} (F)	+1.5	50×10^{-6}	30×10^{-6}	21.5×10^{-6}
	-1.5	20×10^{-6}	380×10^{-6}	200×10^{-6}
	-2.1	500×10^{-6}	16×10^{-6}	7.2×10^{-6}
Y_0 ($S s^{1/2}$)	+1.5	0.07×10^{-3}	0.21×10^{-3}	0.26×10^{-3}
	-1.5	0.05×10^{-3}	0.45×10^{-3}	3×10^{-3}
	-2.1	0.01×10^{-3}	0.8×10^{-3}	0.98×10^{-3}

constant phase element (CPE). The equivalent circuit parameters used for fitting the experimental curves are summarized in

Table 1. The charge-transfer resistance has lower magnitudes under reduction potentials of -1.5 and -2.5 V for PEDOP–Au as compared to neat PEDOP or PEDOP–Ag devices. At -1.5 V, R_{CT} is $50\ \Omega$ for PEDOP–Au, and it increases to $180\ \Omega$ at $E = -2.1$ V. Although the driving force due to applied bias increases, the resistance to ion transfer at the PEDOP–Au/ionic liquid gel interface could probably be due to saturation at the surface of the film. The charge-transfer resistance is also unusually lower than a value of about $6000\ \Omega\ cm^{-2}$ observed for a perfluoro derivative of PEDOT,³⁶ and in another report, for a PEDOT film doped by ClO_4^- ions, it is on the order of $10^2\ \Omega$ under reduction potentials.³⁷ A similar behavior was recorded for the neat PEDOP device as well. Surprisingly, R_{CT} does not change much on going from -1.5 to -2.1 V for the PEDOP–Ag nanocomposite. The relatively smooth surface of PEDOP–Ag in contrast to those of neat PEDOP or PEDOP–Au could be responsible for this digression. A granular, open structure as observed for neat PEDOP or PEDOP–Au (Figure S1a,f in the Supporting Information) provides ion conduction pathways by the virtue of the pores, and this is reflected in the diffusion coefficient values.

$$Z = \left[\frac{1}{Y_0/(j\bar{\omega})^{1/2}} \right] \tanh[B(j\bar{\omega})^{1/2}] \quad (6)$$

$$B = \delta/D^{1/2} \quad (7)$$

From the above relations,³⁸ D was deduced to be $3.1 \times 10^{-7}\ \text{cm}^2\ s^{-1}$ for PEDOP–Au, $2.7 \times 10^{-8}\ \text{cm}^2\ s^{-1}$ for PEDOP–Ag, and $3.9 \times 10^{-9}\ \text{cm}^2\ s^{-1}$ for neat PEDOP, under an oxidation voltage of $+1.5$ V. Only under oxidation potentials was a rather clear Warburg element observed, and therefore, the diffusion coefficient comparison was restricted to only $+1.5$ V. This is larger than the D value on the order of $10^{-10}\ \text{cm}^2\ s^{-1}$ obtained for a PEDOT–Nafion composite³⁹ and also higher than that observed for a zinc hexacyanoferrate–PEDOT:PSS composite ($D \approx 10^{-9}\ \text{cm}^2\ s^{-1}$).⁴⁰ Only for PEDOT nanotubes⁴¹ was a diffusion coefficient of $10^{-6}\ \text{cm}^2\ s^{-1}$, larger than that observed for PEDOP–Au, reported. The double-layer capacitance lies in the range of a few microfarads (C_{dl}) for all three devices and shows a slight dependence on the applied bias (Table 1). Our C_{dl} values agree well with those reported for a PEDOT film doped with perchlorate ions ($20\ \mu\text{F}\ cm^{-2}$)³⁶ and for a PEDOT:PSS film covered by an ionophore ($20–150\ \mu\text{F}$).⁴² In the latter case, C_{dl} was found to vary as a function of the nature and concentration of the electrolyte. Whereas a low R_{CT} value of $30\ \Omega$ was observed for the PEDOP–Au nanocomposite at $+1.5$ V, for PEDOP–Ag, it was $120\ \Omega$, and for neat PEDOP, it was $842\ \Omega$, which is indicative of an easier imide anion deintercalation, assisted by Au nanoparticles in PEDOP–Au. Y_0 , a measure of ease of imide ion insertion and extraction, is higher again for the PEDOP–Au nanocomposite as compared to the other two systems, suggesting that ion propagation through the bulk of the polymer film is facilitated by Au nanoparticles (Table 1). The Bode plots in the insets show that the absolute magnitude of impedance increases at low frequencies because of the diffusional resistance component. The Warburg line shows a $\sim 45^\circ$ inclination only for the PEDOP–Ag nanocomposite under different dc conditions as $\omega \rightarrow 0$, which is evident from the phase angle versus log(frequency) insets.

4. CONCLUSIONS

The role of noble-metal nanoparticles in controlling and promoting charge transport of a conducting polymer, namely, PEDOP, has been demonstrated. Charge transport through the bulk of the polymer is governed by an ohmic dependence at low voltages for all three films, whereas at intermediate voltages, a trap-filled regime was identified in neat PEDOP and PEDOP–Ag in contrast to a distinctive trap-free, space-charge-limited current regime in PEDOP–Au. Further evidence in support of improved pathways of conduction were obtained in terms of macroscopic properties such as 1-fold electronic conductivity and 2-fold donor density increments combined with high charge-carrier mobility for PEDOP–Au as compared to neat PEDOP. Noble-metal nanoparticles, by the virtue of the direct contact they have with the PEDOP, act to decrease the band gap and increase the absorption coefficient, which effectively results in an enhanced electrochromic response. We, therefore, attribute the performance improvement realized for the PEDOP–Au film, in terms of a greater coloration efficiency and a higher charge intercalation/deintercalation capacity during oxidation and reduction to the rapid charge transfer and transport in this film, which is also augmented by an experimentally determined larger diffusion coefficient and smaller charge-transfer resistance.

■ ASSOCIATED CONTENT

S Supporting Information. SEM and AFM images of neat PEDOP, PEDOP–Ag, and PEDOP–Au films; XPS survey scans of neat PEDOP, PEDOP–Ag, and PEDOP–Au films and core-level spectra of nanocomposite films after Ar sputtering; deconvoluted C 1s, O 1s, and S 2p core-level spectra of neat PEDOP, PEDOP–Ag, and PEDOP–Au films; peak positions and atomic percentages from deconvoluted core-level spectra of neat PEDOP, PEDOP–Ag, and PEDOP–Au films; cyclic voltammograms of neat PEDOP, PEDOP–Ag, and PEDOP–Au films in a liquid electrolyte; I – V characteristics of PEDOP–Ag and PEDOP–Au films; absorption spectra of oxidized PEDOP, PEDOP–Au, and PEDOP–Ag films; and cyclic voltammograms of neat PEDOP-, PEDOP–Ag-, and PEDOP–Au-based devices. This information is available free of charge via the Internet at <http://pubs.acs.org>.

■ AUTHOR INFORMATION

Corresponding Author

*Tel.: +91-4023016024. Fax: +91-40-23016003. E-mail: mdeepa@iith.ac.in.

■ ACKNOWLEDGMENT

We thank Mr. Sood for recording SEM images and gratefully acknowledge financial assistance from the Department of Science and Technology (Grant DST/TSG/PT/2007/69).

■ REFERENCES

- (1) Kumar, A.; Welsh, D. M.; Morvant, M. C.; Piroux, F.; Abboud, K. A.; Reynolds, J. R. Conducting poly(3,4-alkylenedioxythiophene) derivatives as fast electrochromics with high-contrast ratios. *Chem. Mater.* **1998**, *10*, 896–902.

- (2) Sonmez, G.; Meng, H.; Wudl, F. Organic polymeric electrochromic devices: Polychromism with very high coloration efficiency. *Chem. Mater.* **2004**, *16*, 574–580.
- (3) Schottland, P.; Zong, K.; Gaupp, C. L.; Thompson, B. C.; Thomas, C. A.; Giurgiu, I.; Hickman, R.; Abboud, K. A.; Reynolds, J. R. Poly(3,4-alkylenedioxyppyrrole)s: Highly stable electronically conducting and electrochromic polymers. *Macromolecules* **2000**, *33*, 7051–7061.
- (4) Sonmez, G.; Schottland, P.; Zong, K.; Reynolds, J. R. Highly transmissive and conductive poly[(3,4-alkylenedioxy)pyrrole-2,5-diyl] (PXDOP) films prepared by air or transition metalcatalyzed chemical oxidation. *J. Mater. Chem.* **2001**, *11*, 289–294.
- (5) Caupp, C. L.; Zong, K.; Schottland, P.; Thompson, B. C.; Thomas, C. A.; Reynolds, J. R. Poly(3,4-ethylenedioxyppyrrole): Organic electrochemistry of a highly stable electrochromic polymer. *Macromolecules* **2000**, *33*, 1132–1133.
- (6) Sih, B. C.; Wolf, M. O. Metal nanoparticle-conjugated polymer nanocomposites. *Chem. Commun.* **2005**, 3375–3384.
- (7) Namboothiry, M. A. G.; Zimmerman, T.; Coldren, F. M.; Liu, J.; Kim, K.; Carroll, D. L. Electrochromic properties of conducting polymer metal nanoparticles, composites. *Synth. Met.* **2007**, *157*, 580–584.
- (8) Li, X.; Li, Y.; Tan, Y.; Yang, C.; Li, Y. Self-assembly of gold nanoparticles prepared with 3,4-ethylenedioxythiophene as reductant. *J. Phys. Chem. B* **2002**, *108*, 5192–5199.
- (9) Yang, W.; Li, J.; Zheng, R.; Liu, Z.; Dai, Y.; Chen, G.; Ringer, S.; Braet, F. Ionic liquid-assisted synthesis of polyaniline/gold nanocomposite and its biocatalytic application. *Nanoscale Res. Lett.* **2008**, *3*, 468–472.
- (10) Cho, S. H.; Park, S. M. Electrochemistry of conductive polymers 39. Contacts between conducting polymers and noble metal nanoparticles studied by current-sensing atomic force microscopy. *J. Phys. Chem. B* **2006**, *110*, 25656–25664.
- (11) Cao, Y.; Kovalev, A. E.; Xiao, R.; Kim, J.; Mayer, T. S.; Mallouk, T. E. Electrical transport and chemical sensing properties of individual conducting polymer nanowires. *Nano Lett.* **2008**, *8*, 4653–4658.
- (12) Mendez, J. D.; Weder, C. Synthesis, electrical properties, and nanocomposites of poly(3,4-ethylenedioxythiophene) nanorods. *Polym. Chem.* **2010**, *1*, 1237–1244.
- (13) Li, W.; Jia, Q. X.; Wang, H. L. Facile synthesis of metal nanoparticles using conducting polymer colloids. *Polymer* **2006**, *47*, 23–26.
- (14) Kharkwal, A.; Deepa, M.; Joshi, A. G.; Srivastava, A. K. Red to blue high electrochromic contrast and rapid switching poly(3,4-ethylenedioxyppyrrole)-Au/Ag nanocomposite devices for smart windows. *ChemPhysChem* **2011**, *12*, 1176–1188.
- (15) He, R.; Qian, X.; Yie, J.; Zhu, Z. Preparation of polychrome silver nanoparticles in different solvents. *J. Mater. Chem.* **2002**, *12*, 3783–3786.
- (16) Jiang, Y.; Shen, Y.; Wu, P. Self-assembly of multilayer films containing gold nanoparticles via hydrogen bonding. *J. Colloid Interface Sci.* **2008**, *319*, 398–405.
- (17) Bhandari, S.; Deepa, M.; Pahal, S.; Joshi, A. G.; Srivastava, A. K.; Kant, R. A. Dual Electrochrome of Poly-(3,4-ethylenedioxythiophene) Doped by *N,N'*-Bis(3-sulfonatopropyl)-4,4'-bipyridinium Redox Chemistry and Electrochromism in Flexible Devices. *ChemSusChem* **2010**, *3*, 97–105.
- (18) Deepa, M.; Awadhia, A.; Bhandari, S. Electrochemistry of poly(3,4-ethylenedioxythiophene)-polyaniline/Prussian blue electrochromic devices containing an ionic liquid based gel electrolyte film. *Phys. Chem. Chem. Phys.* **2009**, *11*, 5674–5685.
- (19) Mikalo, R. P.; Appel, G.; Hoffmann, P.; Schmeisser, D. Band bending in doped conducting polypyrrole: Interaction with silver. *Synth. Met.* **2001**, *122*, 249–261.
- (20) Hwang, J.; Amy, F.; Kahn, A. Spectroscopic study on sputtered PEDOT · PSS: Role of surface PSS layer. *Org. Electron.* **2006**, *7*, 387–396.
- (21) Beaujuge, P. M.; Amb, C. M.; Reynolds, J. R. Spectral engineering in π -conjugated polymers with intramolecular donor–acceptor interactions. *Acc. Chem. Res.* **2010**, *43*, 1396–1407.
- (22) Chen, C.-H.; Hsieh, C.-H.; Dubosc, M.; Cheng, Y. J.; Hsu, C.-S. Synthesis and characterization of bridged bithiophene-based conjugated polymers for photovoltaic applications: Acceptor strength and ternary blends. *Macromolecules* **2010**, *43*, 697–708.
- (23) Thomas, C. A.; Zong, K.; Abboud, K. A.; Steel, P. J.; Reynolds, J. R. Donor-mediated band gap reduction in a homologous series of conjugated polymers. *J. Am. Chem. Soc.* **2004**, *126*, 16440–16450.
- (24) Bisquert, J.; Garcia-Belmonte, G.; Munar, A.; Sessolo, M.; Soriano, A.; Bolink, H. J. Band unpinning and photovoltaic model for P3HT:PCBM organic bulk heterojunctions under illumination. *Chem. Phys. Lett.* **2008**, *465*, 57–62.
- (25) Şahingöz, R.; Kanbur, H.; Voigt, M.; Soykan, C. The determination of interface states and series resistance profile of Al/polymer/PEDOT-PSS/ITO heterojunction diode by I–V and C–V methods. *Synth. Met.* **2008**, *158*, 727–731.
- (26) Carbone, A.; Kotowska, B. K.; Kotowski, D. Space-charge-limited current fluctuations in organic semiconductors. *Phys. Rev. Lett.* **2005**, *95* (236601), 1–4.
- (27) Nicolai, H. T.; Wetselaer, G. A. H.; Kuik, M.; Kronemeijer, A. J.; de Boer, B.; Blorn, P. W. M. Space-charge limited hole current in poly(9,9-diethylfluorene) diodes. *Appl. Phys. Lett.* **2010**, *97* (172107), 1–3.
- (28) Reid, O. G.; Munechika, K.; Ginger, D. S. Space charge limited current measurements on conjugated polymer films using conductive atomic force microscopy. *Nano Lett.* **2008**, *8*, 1602–1609.
- (29) Li, H.; Lambert, C.; Stahl, R. Conducting Polymers Based on Alkylthiopyrroles. *Macromolecules* **2006**, *39*, 2049–2055.
- (30) Garcia-Belmonte, G.; Munar, A.; Bareja, E. M.; Bisquert, J.; Ugarte, I.; Pacios, R. Charge carrier mobility and lifetime of organic bulk heterojunctions analyzed by impedance spectroscopy. *Org. Electron.* **2008**, *9*, 847–851.
- (31) Winther-Jensen, B.; Forsyth, M.; West, K.; Andreasen, J. W.; Wallace, G.; MacFarlane, D. R. High current density and drift velocity in template conducting polymers. *Org. Electron.* **2007**, *8*, 796–800.
- (32) Kan, C.; Wang, C.; Zhu, J.; Li, H. Formation of gold and silver nanostructures within polyvinylpyrrolidone (PVP) gel. *J. Solid State Chem.* **2010**, *183*, 858–865.
- (33) Lin, T.-H.; Ho, K.-C. A complementary electrochromic device based on polyaniline and poly(3,4-ethylenedioxythiophene). *Sol. Energy Mater. Sol. Cells* **2006**, *90*, 506–520.
- (34) Tung, T.-S.; Ho, K.-C. Cycling and at-rest stabilities of a complementary electrochromic device containing poly(3,4-ethylenedioxythiophene) and Prussian blue. *Sol. Energy Mater. Sol. Cells* **2006**, *90*, 521–537.
- (35) Gaupp, C. L.; Welsh, D. M.; Rauh, R. D.; Reynolds, J. R. Composite coloration efficiency measurements of electrochromic polymers based on 3,4-alkylenedioxythiophenes. *Chem. Mater.* **2002**, *14*, 3964–3970.
- (36) Benedetto, A.; Balog, M.; Rayah, H.; Derf, F. L.; Viel, P.; Palacin, S.; Sallé, M. Fluorinated functionalized EDOT-based conducting films. *Electrochim. Acta* **2008**, *53*, 3779–3788.
- (37) Hass, R.; García-Cañadas, J.; García-Belmonte, G. Electrochemical impedance analysis of the redox switching hysteresis of poly(3,4-ethylenedioxythiophene) films. *J. Electroanal. Chem.* **2005**, *577*, 99–105.
- (38) MacDonald, J. R. *Impedance Spectroscopy: Emphasizing Solid Materials and Systems*; Wiley-Interscience, 1987.
- (39) Wang, P.; Olbricht, W. L. PEDOT/Nafion composite thin films supported on Pt electrodes: Facile fabrication and electrochemical activities. *Chem. Engng. J.* **2010**, *160*, 383–390.
- (40) Hong, S.-F.; Chen, L.-C. A red-to-gray poly(3-methylthiophene) electrochromic device using a zinchexacyanoferrate/PEDOT:PSS composite counter electrode. *Electrochim. Acta* **2010**, *55*, 3966–3973.
- (41) Abidian, M. R.; Martin, D. C. Experimental and theoretical characterization of implantable neural microelectrodes modified with conducting polymer nanotubes. *Biomaterials* **2008**, *29*, 1273–1283.
- (42) Lisowska-Oleksiak, A.; Lesińska, U.; Nowak, A. P.; Bocheńska, M. Ionophores in polymeric membranes for selective ion recognition; impedance studies. *Electrochim. Acta* **2006**, *51*, 2120–2128.